LBL--14142

DE83 005067

Submitted for presentation at the 1983
Particle Accelerator Conference, Santa Fe,
New Mexico, March 21-23, 1983

TRAVELING-WAVE TUBE AMPLIFIER CHARACTERISTICS STUDY FOR STOCHASTIC BEAM-COOLING EXPERIMENTS

Branko Leskovar and C. C. Lo

Lawrence Berkeley Laboratory
University of California
Department of Instrument Science and Engineering
Electronics Research and Development Group
Berkeley, California 94720 U.S.A.

March 4, 1982

Prepared for the U. S. Department of Energy
Under Contract DE-AC03-76SF00098

TRAVELING-WAVE TUBE AMPLIFIER CHARACTERISTICS STUDY FOR STOCHASTIC BEAM COOLING EXPERIMENTS

LBL-14142

Branko Leskovar and C.C. Lo

Lawrence Berkeley Laboratory
University of California
Berkeley, California 94720 U.S.A.

Summary

The characteristics of continuous-wave wideband traveling-wave tube amplifiers have been experimentally investigated over a frequency range of 1.5 to 4.5 GHz. We present measurements of characteristics important for stochastic beam cooling systems that are generally not available from manufacturers' data sheets. The amplifers measured include models 1177 HOI and 1277 HOI having output power capabilities of 10 to 20 W, respectively, at frequencies of 2 to 4 GHz. The power transfer characteristics, the phase-shift characteristics as functions of frequency and the input power level, the voltage standing-wave ratio, noise drive transfer characteristics, harmonics and intermodulation products content were accurately measured and are discussed. Measurement procedures and description of measuring systems, which include measuring system error corrections, are given in detail. Also several approaches are discussed for the reduction of harmonics and intermodulation products.

Introduction

An effort is underway at the Fermi National Accelerator Laboratory and Lawrence Berkeley Laboratory to design the Antiproton Source which will make it possible to produce proton-antiproton collisions at energies near 2 TeV in the center of mass.[1] The Antiproton source will be capable of accumulating 4×10^{11} antiprotons in four hours when a wideband feedback system[2,3] for stochastic beam cooling is used. This method has been effectively used for the gradual reduction of betatron oscillations and longitudinal momentum spread of a coasting particle beam. The method is essential in order to achieve a high luminosity proton-antiproton colliding beam facility.[4]

The feedback system detects and corrects at every revolution, the statistical fluctuations of the beam position or momentum. It typically consists of a wideband pickup electrode, able to detect horizontal or vertical statistical displacements of short samples of a coasting beam, low-noise wideband power amplifiers and kicker electrodes which apply correcting signals to the same beam sections sampled. To reduce the longitudinal momentum spread, the system consists of radial differences pickup electrodes which observe the error in the radial position of the barycentre of short samples of the beam with respect to their nominal radial positions, low-noise wideband power amplifiers and wideband accelerating gaps. The error signal generated by a pickup electrode is interpreted as a momentum error, and a fraction of it is corrected by amplifying the signal and applying it to the gap at the instant the sampled portion of the beam passes. In general, theoretical considerations and experimental results of stochastic cooling have shown that the effective cooling rate is limited by the system bandwidth, the noise figure, the beam Schottky noise, system gain, the power level available to kicker electrode, the particle mixing process, imperfect components and undesirable system phase shift errors.[5-8]

In the Debuncher Ring of the Antiproton Source the antiproton betatron oscillations will be reduced by a low-noise low power amplifier system having a frequency range of 2 to 4 GHz. In the Accumulator Ring of the Antiproton Source the low density stack of antiprotons will be stochastically cooled using a stack-tail cooling system similar to the type developed for the CERN Antiproton Accumulator.[9] This system will use a low-noise medium power amplifier with covering a frequency band 1-2 GHz. The high density antiproton region will be cooled by stack-core cooling systems, consisting of low-noise low-power amplifier with the bandwidth of 4-8 GHz. Later, systems with a bandwidth covering 4-8 GHz will be used if future research and development efforts indicate that large bandwidth cooling systems are practical.

The Antiproton Source program requires the development of two types of wideband amplifier systems, one type capable of operating at power levels of several hundred watts and the other at power levels of several thousand watts in the frequency bandwidths covering 1-2 GHz and 2-4 GHz. Since the pickup electrodes generate very small signal power levels from the antiproton beam amplifier systems should have a gain in excess of 90 dB and 150 dB, and noise figures as low as possible. Furthermore, the systems should have accurately controllable signal propagation time delays. Also, the propagation time change as a function of the system gain settings, harmonics and intermodulation distortions should be minimized.

Our previous experiments[10,11] and considerations[12] indicate that new amplifier systems should be designed which meet the above requirements for fast cooling of betatron oscillations and longitudinal momentum spread. The characteristics of the amplifier systems will be limited by the capabilities of available individual state-of-the-art components, particularly the amplifier driver and output power stages. Initially Power Gallium-Arsenide Field-Effect Transistors and Helix Traveling-Wave Tubes (TWT) were considered as potential devices for the amplifier driver and output stages. Detailed device characteristics studies have shown that at the present time only helix-type TWT's are capable of meeting the technical objectives at output power level, bandwidth, phase-shift variations, and reliability.[13] Because of the TWT's excellent gain bandwidth and output power capabilities,[14,15] the device can significantly contribute to the development of stochastic cooling systems. However, device characteristics must be carefully studied, particularly with respect to generation of harmonics and intermodulation products during amplification process. Harmonics and intermodulation products are generated as a result of the inherent nonlinearity of the beam-helix wave interaction process in TWT's when multiple

input signals (or noise) are applied. The generation of such harmonics and intermodulation products in the amplifier system may cause the stochastic heating rather than cooling of antiproton beam.

This paper presents and discusses characteristics of Hughes 1177 H01 and 1277 H01 TWT amplifiers, having output power capabilities of 10 to 20 W, respectively, in a bandwidth covering 2 to 4 GHz. Measurement of characteristics, important for stochastic beam cooling systems and generally not available from manufacturers' date sheets, include the power transfer and phase-shift characteristics as functions of frequency and input power level, the input and output voltage standing-wave ratio, harmonics and the intermodulation products content.

A schematic arrangement of the TWT amplifier is shown in Fig. 1. Amplification is provided in the device by causing an electromagnetic wave to travel along a helical slow-wave structure in close proximity with an electron beam. A focusing device is used to confine the beam in the slow-wave structure. The RF signal to be amplified is applied to helix input and travels along the helix at approximately the same velocity as the electron beam. As the beam moves through the helix electrons form bunches. These bunches are actually RF current pulses which induce a corresponding voltage in the slow-wave structure amplifying the input signal. The amplified signal then reacts further on the electron beam and causes more effective bunch formation. In this way, the input signal is amplified on the slow-wave structure until it is finally emerges at the helix output connector. Generally, the high gain TWT has an internal attenuator to avoid the amplification of reflections and subsequent oscillations.

Instrumentation Power Amplifiers 1177 H01 and 1277 H01 have TWT's model numbers 564H and 568H, respectively. Both TWT's have no modulating grids in the tube electron gun region.

Dynamic Range and Power Transfer Characteristics Measurement

The dynamic range measurement of the TWT amplifier show performance characteristics such as linearity and gain. A block diagram of the system used for dynamic range and power transfer characteristics measurement is given in Fig. 2. Approximately 100 mW of signal power was required to drive the TWT amlifier under test to provide full power output and operate beyond the saturation. The output signal from a signal generator is attenuated by two precision wideband attentuators before it is amplified by a wideband preamplifier. This wideband power divider at the output of the preamplifier divided the signal into two equal parts. One part was used for monitoring purposes: a power meter or a spectrum analyzer being used for this function. The other part was used to drive the TWT amplifier under test. At the time of testing a high power widehand attenuator was not available, hence a directional coupler with a high power 50 ohm termination was used to monitor the output of the TWT amplifier. A spectrum analyzer with a preselector was used to measure the output signal.

Figure 3 shows the output power of the TWT amplifier as a function of the input power level with the input signal frequency as a parameter. The 1.0, 1.5 and 4.5 GHz signals were beyond the specified 2-4 GHz bandwidth of the amplifier. Results of the measurements show that the amplifier has its 1 dB compression point at output power level of 40, 42 and 45 dBm for frequencies of 3, 2 and 4 GHz, respectively. Saturation points were 45, 42 and 45 dBm for input signal frequencies of 3, 2 and 4 GHz. Figure 4 shows the output power as a function of the signal frequency with the input power level as a parameter. The output power variation across the specified bandwidth was approximately 12 dB. As the input power approached 0 dBm, the output power curve showed a marked saturation. The linear operating range of the TWT amplifier was definitely below 0 dBm of input power over the 1.5-4 5 GHz range. The output noise power level of the TWT was -55 dBm. For this measurement the spectrum analyzer bandwidth was 300 KHz.

The amplifier gain as a function of frequency is shown in Fig. 5. The measurement was made using a network analyzer. The frequency range was from 1.8 to 4.2 GHz. The gain curve shows periodic variations of ± 3 dB at 3 GHz, in addition to a large gain variation of approximately 20 dB through the measuring frequency band.

Phase-Shift Characteristics Measurement

The phase-shift characteristics of the TWT amplifier are important for proper operation of the wideband feedback cooling system both from the standpoint of overall system stability and making an estimate of the phase-shift error between the pickup and kicker electrode signals. Too great a phaseshift error causes heating rather than cooling of the antiproton beam. The phase-shift characteristic was measured using the measuring system shown in Fig. 6. The test signal generation section is similar to one shown in Fig. 2. The signal from one part of the power divider was used for monitoring purposes: in this case a spectrum analyzer was used. The signal from the other part of the divider was connected to a reflection/transmission test unit which was part of the network analyzer system.

Before the phase measurement of the TWT amplifier was made, the measuring system phase characteristic was measured. This was done by replacing the TWT amplifier with a short piece of high quality cable which had the same signal propagation delay time as the TWT amplifier. For this particular TWT amplifier, the signal propagation time was 9.5 ns. The system phase characteristic was mainly that of the directional coupler. The amount of system phase shift must be subtracted from the total phase shift to obtain the phase characteristics of the TWT amplifier.

Figure 7 is a set of curves showing the phase-shift of the TWT amplifier output signal as a function of frequency at various input power levels. The measuring system phase-shift had been subtracted and this figure presents the true phase-shift of the TWT amplifier output with zero phase set at 2.5 GHz and -10 dBm input power level. The amount of phase-shift over a bandwidth of 2-4 GHz at 0 dBm input power level was ± 30°. At input power level of -10 dBm, the phase-shift was ± 21°.

Figure 8 shows the amplifier and system phase characteristic with an input power level of -10 dBm. The phase-shift was not only due to the TWT amplifier, but was contributed to by the directional coupler, the cables, connections, and the instruments used. The total phase shift across the 1.8-4.2 GHz frequency band with an input power level of -10 dBm was ± 36°.

Figure 9 is the phase-shift of the TWT amplifier as a function of input power level with input signal frequency as parameter. The 2, 3 and 4 GHz curves are all normalized with respect to each other through a zero-phase set point fixed at 2.5 GHz and -10 dBm input power level. For the input power dynamic range from 0 to -20 dBm, the phase-shift as a function of the input power level varies 2, 7 and 45° for the input signal frequencies of 4, 2 and 3 GHz, respectively.

Dynamic Range and Intermodulation Products Measurement

The dynamic range and intermodulation product measurement of the TWT amplifier shows such performance characteristics as the linearity, gain, harmonic interference, and the intermodulation performance which can be expected from the amplifier at certain specified frequencies. As a result of the inherent nonlinearity of the electron beam-helix wave interaction process, harmonics and intermodulation products are formed when multiple input signals (or noise) are applied which reduce the available power levels of the fundamental signals. Distortion and nonlinear effects are caused by electron bunching, velocity modulation, and electrons overtaking in the beam. Distributed helix loss, variation of tube parameters with frequency and space-charge force phenomena also contribute.[16,17] It was also shown that the presence of attenuators for the supression of oscillations can significantly influence nonlinearity in the traveling-wave tubes.[18]. Generally, when two input signals with frequencies f_1 and f_0 are applied to the TWT amplifier the frequency of the intermodulation signal is $mf_1 \pm nf_0$, where m and n are positive integers. One of the integers may take the value zero so that harmonics are included. The order of the general intermodulation products is given by the sum of the integers m + n. Figure 10 shows a block diagram of the measuring system. Two signal generators were used for intermodulation measurements. Two pairs of sample frequencies were used in the measurement namely: 1.8 and 2 GHz and 3 and 3.2 GHz. An in-phase power combiner added the two separate signals together to produce the two carrier signal. Two precision wideband attenuators provide 1 and 10 dB steps of attenuation.

Before the two carrier signal was used to drive the TWT amplifier it was observed on the spectrum analyzer to determine its own harmonics and intermodulation product content. With power level set at 5 dBm for both signals which was the maximum input power level used for the measurement, the harmonics, intermodulation products as well as the mixing sum and difference of the signals were all 35 dB or more below the main signal levels. The dynamic range of the TWT amplifier operating with a two carrier signal was lower than that of single signal operation.

In Fig. 11, the output power of the two main carriers and some of their harmonics and intermodulation products are plotted as a function of the main carrier's input power. The two signal frequencies 1.8 and 2 GHz were chosen because the second harmonics, the sum and difference of the signals and third order intermodulation products are mostly in the pass band of the amplifier. The two carriers were designated as f_1 (2 GHz) and f_0 (1.8 GHz). At 0 dBm input power level, the sum of f_1 and f_0 was less than 5 dB below the carriers and the second harmonics were less than 10 dB below the carriers. At +5 dBm input power level, the $f_1 + f_0$ component actually had a higher output than the 1.8 GHz carrier. Even at -10 dBm input power level, the second harmonics and the $f_1 + f_0$ component were less than 20 dB below the carrier's output power levels which were, at this point, 1 W and 0.5 W, respectively, for f_1 and f_0. In Fig. 11 all presented data were corrected for the measuring system errors.

Figures 12, 13, 14, and 15 show frequency spectra of the TWT amplifier output at input power levels of 0 dBm and -10 dBm. Figure 12 shows all the components from 1.5 to 3.55 GHz. Figure 13 shows all the components between 2.07 and 6.17 GHz. It is interesting to note that the four components 5.4, 5.6, 5.8 and 6 GHz are all beyond the frequency passband of the amplifier. As a matter of fact the TWT amplifier attenuates signals in this frequency range. The 6 GHz component is $3f_1$, 5.4 GHz is $3f_0$, 5.8 GHz is $2f_1 + f_0$ and 5.6 GHz is $2f_0 + f_1$. The amplifier did not behave like an amplifier any more in this frequency range. A low pass filter was used at the input and output to confirm the presence of these components.

Figures 14 and 15 show corresponding spectra at -10 dBm input power levels.

Figure 16 shows the results of a similar measurement taken with f_1 = 3 GHz and f_0 = 3.2 GHz. The second harmonic and the third order intermodulation products were approximately 15 dB below the carrier at an input power level of 0 dBm. Figures 17, 18 and 19, 20 show the frequency spectra of the TWT amplifier output at input power levels of 0 dBm and -10 dBm, respectively.

This frequency spectra exhibits a behavior similar to that in the previous case. However, the amplitude of the $2f_0 - f_1$ and $2f_1$ components is smaller than for the pair of sample frequencies at 1.8 and 2 GHz

Voltage Standing-Wave Ratio Measurements

The input and output Voltage Standing-Wave Ratio, VSWR, were measured across the 1.8 - 4.5 GHz frequency range. A network analyzer was used for this measurement. The results of the measurements are shown in Fig. 21. The maximum VSWR of the input was less than 2.0, while the maximum output VSWR was less than 2.2.

Amplifier Transfer Characteristics Measurements Using the Wide-Band Input Noise

The application of wide-band noise to the input of TWT amplifier was also investigated. Of particular interest is the amplifier transfer characteristics under noise drive compared with the results when there is only a single frequency input signal.

The noise figures of the TWT measured in this laboratory were approximately 30 dB - a common value for this class of medium power tubes. The output noise power level was -13 dBm, measured with the input of TWT amplifier terminated by 50 Ohms and using power meter with a 0.01 - 18 GHz bandwidth. Most of the output power was in the portion of the frequency spectrum between the 1.5 - 4.5 GHz. The amplifier output noise power as a function of the input noise power level was measured with a solid state noise source and three 1.0 - 4.5 GHz solid

state amplifiers. Results are shown in Fig. 22. The 1 dB compression point for the 20 W amplifier is at 44 dBm and thus is 57 dB above the noise level.

In the second test the spectrum of the input noise was modified by a notch filter and resulting output harmonics and intermodulation products introduced by the TWT amplifier were measured. For this purpose notches with 270 MHz frequency separation were obtained by using two matched adjustable 270 MHz stubs and DC-18 GHz power splitters. Such a combination forms two identical notch filters connected in series. The resultant notch depth in this input signal was of the order of 45 dB in the 1-4.5 GHz frequency band. Figure 23 shows the TWT amplifier input noise spectrum having notches at 1.32 GHz, 1.59 GHz and 1.86 GHz. *Figure 24 shows the amplifier output noise spectrum* between 2.5 and 3.5 GHz at output power level of +26 dBm, (measured by a wideband power meter). Because of the harmonics, and intermodulation products generated in the amplifier, the depths of the notches of the output noise spectrum were reduced to 36 dB, or 9 dB less than those in the input noise spectrum. *Figure 25 shows the amplifier output noise spectrum* between 3.5 and 4.5 GHz, at the output power level being +26 dB. The depth of the 4 GHz notch in the output noise spectrum was reduced to 25 dB, or 20 dB less than those in the input noise spectrum. Generally, the decrease of the notch depths of the output spectrum rises rapidly beyond an output power level of +30 dBm.

During this measurement, the input noise signal level going into the preselector - spectrum analyzer system was, at all times, kept below 0 dBm to avoid the signal compression effect. It should be pointed out that the noise level of the spectrum analyzer sets a lower limit to the usable signal level below which the true notch depth is masked by noise. These two limitations introduce an error in measuring the notch depth especially at the two ends of the frequency band.

Conclusions

Experimental studies on several low power continuous-wave wideband TWT amplifiers have been presented and discussed. Wideband TWT amplifiers with low and medium output power levels are becoming a key component for future stochastic beam cooling systems. The performance characteristics of TWT's will primarily determine the effectiveness and cost of these systems. When properly used, the important performance parameters that these devices must have are: large bandwidth and dynamic range, high output power level, good phase-shift characteristics with respect to input signal frequency and power level, and a reasonable degree of nonlinearity (or low content of harmonics and intermodulation distortion under multi-frequency input signal operation). For maximum obtainable efficiency from TWT's, they should be operated at or close to saturation. However, in this operating region, the device characteristics became rather nonlinear and exhibit sizable distortion. Our measurements show that in addition to second harmonics, third order intermodulation products ($2f_1-f_0$, $2f_0-f_1$), and fifth order intermodulation products ($3f_1-2f_0$, $3f_0-2f_1$), strong sum-and-difference components ($f_1 \pm f_0$) are present in the output signal. Generally, in the quasi-linear or small input region the rate of increase of the second harmonic and sum-and-difference components is approximately twice that of the fundamental signal. The rate of increase of the third order intermodulation products is approximately three times larger than the fundamental signal increase rate. Linearity requirements of the stochastic beam cooling systems, with respect to harmonics, sum-and-difference components and intermodulation products generation during amplification process, can be met by an output power backoff from the saturation point and applications of amplitude and phase pre-distorting networks together with feedforward techniques. Optimization of the TWT operating conditions could reduce the device distortion. Furthermore, the possibility should be explored of developing a special TWT having improved amplitude linearity with respect to those commonly available. The design of standard TWT's by manufacturing industry has, in most cases, emphasized power efficiency, output power levels, bandwidth, gain, size, reliability rather than amplitude linearity. For stochastic beam cooling systems, the emphasis should be on amplitude linearity, bandwidth and reliability, sacrificing to some extent power efficiency and gain. The amplitude linearization of the TWT would also result in an improvement in phase linearity.

The required output power level of the octave-bandwidth amplifier for the stochastic cooling systems can be obtained by either a large number of low power CW Traveling-Wave Tubes (200 W saturated power level) or a relatively small number of medium power TWT's (1.5 kW saturated power). The use of low power TWT's *rather than medium power tubes has the following* advantages: higher reliability, availability of the tubes from at least three major manufacturers, willingness of one manufacturer to redesign the TWT to reduce harmonic and intermodulation product output, and a better output power-to price ratio ($100/W for 200 W tube versus $220/W for 1.5 kW tube). The octave bandwidth CW medium power TWT's are available only from one major manufacturer which presently is not willing to make any tube modification for reduced harmonic and intermodulation products output. Mean-Time-Between-Failure (MTBF) of 200 W TWT's is, approximately, between 15,000 and 20,000 hours. The 1.5 kW TWT's has MTBF of approximately 3,000-5,000 hours. With a high redundancy design, the reliability of a 200 W TWT system can be significantly higher than that of a 1.5 kW TWT system.

Concerning the configuration of high power TWT's in the output stage, the TWT's can be reliably used only as single units in the octave bandwidth. Although, the operation of several TWT's in parallel configuration is possible for obtaining higher power levels, it requires a complex protection circuitry, careful phase and amplitude matching and precise maintenance of the matching conditions over the operational lifetime of the output stage. So far, parallel configuration of TWT's has been used exlusively in military electronic counter measure systems, in the octave bandwidth, purely to increase the output power level. It cannot be used to reduce the harmonics and intermodulation product content due to a complex interaction of beam-helix wave in TWT's.

In satellite communication applications where requirements are more stringent in terms of amplitude, phase linearity and gain stability (to some extent similar to stochastic cooling system requirements) the parallel combination of two TWT's has been used only for relatively narrow (8%) bandwidths. Specifically, a satellite earth terminal was developed *which is capable of delivering 1 kW CW in a bandwidth* extending from 5.9 GHz to 6.4 GHz (C-Band) by combining two 600 W TWT's and using precision type

input and output components.[19] At X-Band frequencies the satellite communication systems successfully use only 5% bandwidths. The relatively narrow operational bandwidths in both cases was essentially determined by the accuracy of phase tracking in all precision components used in the system, such as the input in-phase power splitters, attenuators, phase-shifters, the TWT's and the output in-phase power combiners.

Single TWT configuration in the output stage would eliminate the precise amplitude and phase matching requirements over the required large bandwidth and output signal dynamic range. Furthermore, such a configuration will allow freedom in optimizing the operating conditions of each tube in the system, as well as the application of amplitude and phase predistorting networks and feed-forward techniques.

Acknowledgment

This work was performed as part of the program of the Electronics Research and Development Group and the Advanced Accelerator Group of the Lawrence Berkeley Laboratory, University of California, Berkeley, and was supported by the Office of High Energy and Nuclear Physics of the U.S. Department of Energy under Contract No. DE-AC03-76SF00098.

Reference to a company or product name does not imply approval or recommendation of the product by the University of California or the U.S. Department of Energy to the exclusion of others that may be suitable.

References

1. The Fermi Laboratory Antiproton Source Design Report, Fermi National Accelerator Laboratory, Batavia, IL, February 1982.

2. H.G. Hereward, Statistical Phenomena-Theory, Proc. of the First Course of the International School of Particle Accelerators, Erice, 1976, CERN 77-13, 281-289 (July 1977).

3. W. Schnell, Statistial Phenomena-Experimental Results, Proc. of the First Course of the International School of Particle Accelerators, Erice 1976, CERN 77-13, 290-313 (July 1977).

4. D. Möhl, Stochastic Cooling, European Organization for Nuclear Research Report, CERN/PS/OL 78-25 (October 1978).

5. G. Carron, H. Herr, G. Lebee, H. Koziol, F. Krienen, O. Möhl, G. Petrucci, C. Rubbia, F. Sacherer, G. Sadoulet, G. Stefanini, L. Thorndahl, S. van der Meer, T. Wikberg, Experiments on Stochastic Cooling in ICE, Report CERN-EP-179-16, March 1, 1979. Particle Accelerator Conf., San Francisco, March 12-14, 1979, IEEE Trans. Nucl. Sci. NS-26, 3456-3461 (1979).

6. S. van der Meer, Stochastic Cooling Theory and Devices, Proc. of the Workshop on Producing High Luminosity High Energy Proton-Antiproton Collisions, March 27-31, 1979, Berkeley, California. Lawrence Berkeley Laboratory Report, LBL-7574, UC-34C, CONF-780345, pp. 73-77 (1979).

7. G. Carron, H. Herr, H. Koziol, F. Krienen, D. Möhl G. Petrucci, C. Rubbia, F. Sacherer, B. Sadoulet, L. Thorndahl, S. van der Meer, T. Wikberg, Stochastic Cooling Tests in ICE Phys. Let., 77B, No. 3 (August 1978).

8. F.J. Sacherer, Stochastic Cooling Theory, CERN-ISR-TH/78-11 (1978).

9. S. van der Meer, Stochastic Stacking in the Antiproton Accumulator, CERN/PS/AA/78-22 (1978).

10. G. Lambertson, J. Bisognano, W. Flood, F. Laslett, C Leemann, B. Leskovar, C.C. Lo, R. Main, L. Smith J. Staples, Stochastic Cooling of 200 MeV Protons, Proc. of the 11th Int. Conf on High-Energy Accelerators, Geneva, Switzerland, pp. 794-799, July 1980. Experientia Supplementum, Vol. 40, Birkanser Verlag, Basel, Switzerland.

11. G. Lambertson, J. Bisognano, W. Flood, K. Kim, C. Leeman, B. Leskovar, C.C. Lo, R. Main, R. Rimers, L. Smith, J. Staples, Experiments on Stochastic Cooling of 200 MeV Protons, IEEE Trans. Nucl. Sci. NS-28, No. 3, 2471-2473, (1981).

12. B. Leskovar, C.C. Lo, Low-Noise Wide-Band Amplifier System for Stochastic Beam Cooling Experiments, IEEE Trans. Nucl. Sci. NS-27, No. 1, 292-301 (1980).

13. B. Leskovar, Reliability Considerations of Traveling Wave Tube and Power Gallium Arsenide Field-Effect Transistor Amplifiers, Lawrence Berkeley Laboratory Report No. LBL-13861, (1981).

14. J.T. Mendel, Helix and Coupled-Cavity Traveling Wave Tubes, Proc. of the IEEE, 61, No. 3, 280-298 (March 1973).

15. R. Strauss, J. Bretting, R. Metivier, Traveling Wave Tubes for Communication Satellites, Proc. of the IEEE, 65, No. 3, 387-400 (March 1977).

16. J.L. Putz, Predicting Nonlinear Effects in TWT's, Microwaves 4, 32-39 (June 1965).

17. M.K. Scherba, J.E. Rowe, Characteristics of Multisignal and Noise-Modulated High-Power Microwave Amplifiers, IEEE Trans. Elec. Devices, ED-18, No. 1, 11-34, (1971).

18. J. Ober, The Large Signal Behavior of a Traveling Wave Tube with an Attenuating Central Helix Section, Philips Res. Reports, 20, 357-376 (1965).

19. R.E. Shuken, Paralled TWT's Boost Uplink Power, Microwave Systems News, 7, 55-60, (1977).

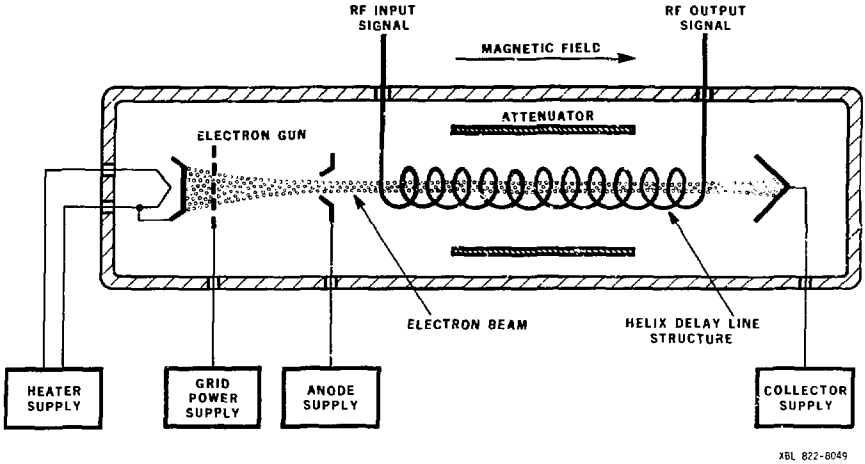

Fig. 1 Schematic arrangement of a traveling-wave tube amplifier.

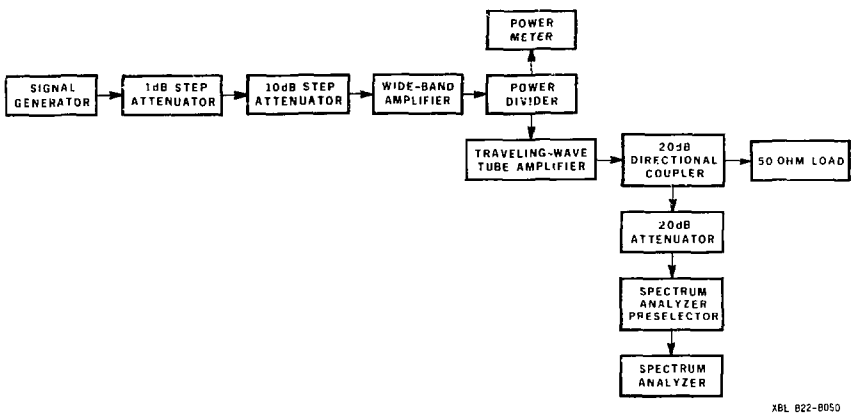

Fig. 2 System block diagram for dynamic range and power transfer characteristics measurement.

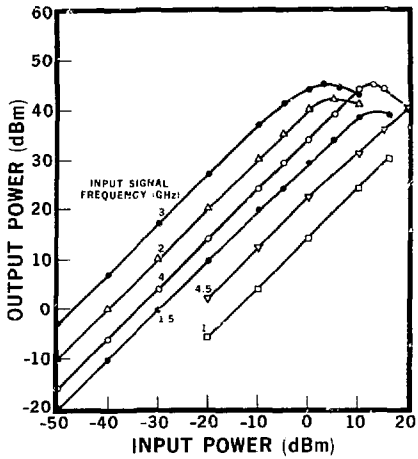

Fig. 3 Output power as a function of the input power level with the input signal frequency as parameter.

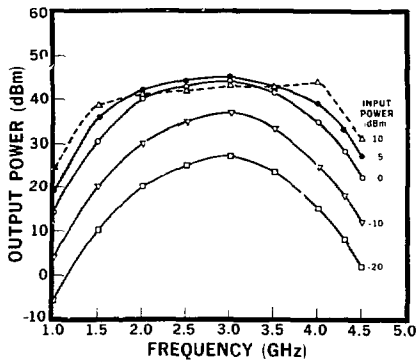

Fig. 4 Output power as a function of frequency with the input power level as parameter.

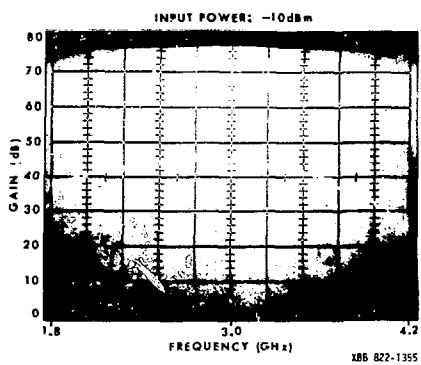

Fig. 5 Gain as a function of frequency of the traveling-wave tube amplifier.

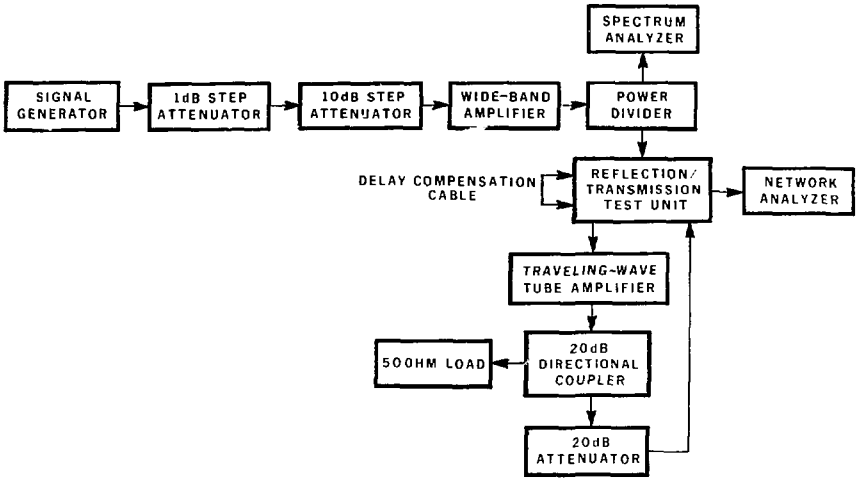

Fig. 6 Block diagram of the system for measuring amplifier phase-shift characteristics.

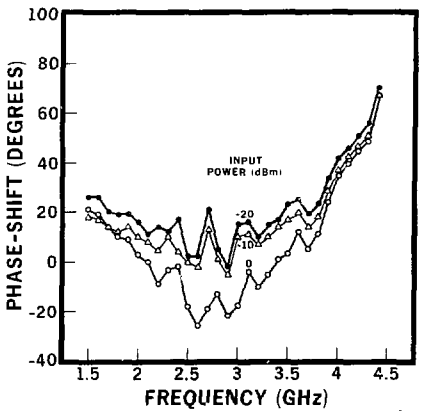

Fig. 7 Amplifier phase-shift as a function of frequency with the input power level as parameter.

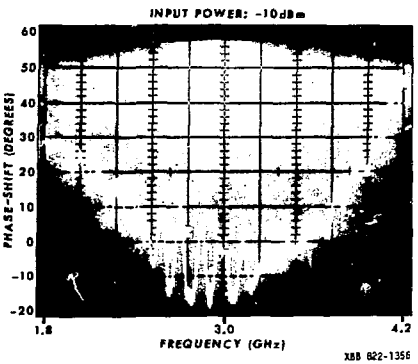

Fig. 8 Amplifier phase-shift characteristics.

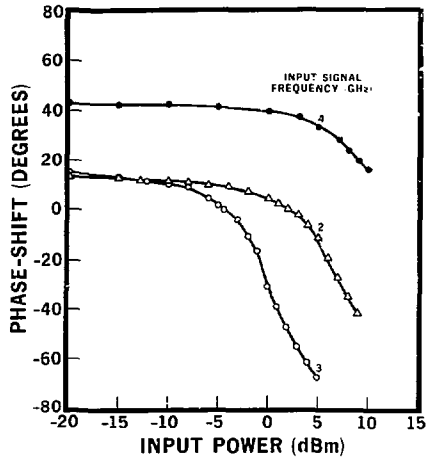

Fig. 9 Amplifier phase-shift characteristics as a function of the input power level with input signal frequency as parameter.

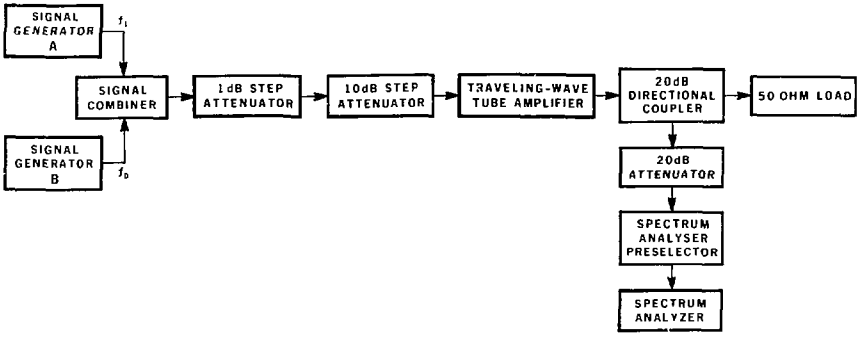

Fig. 10 System block diagram for dynamic range and intermodulation product measurements.

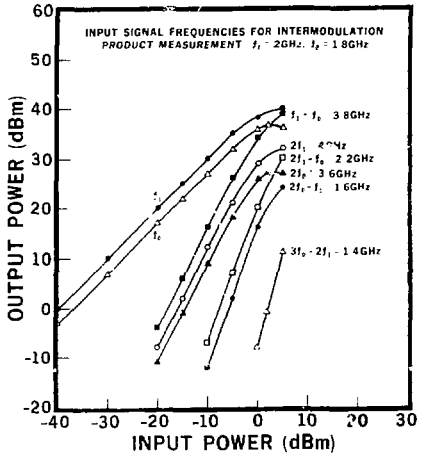

Fig. 11 Typical performance characteristics of the 2-4 GHz traveling-wave tube amplifier.

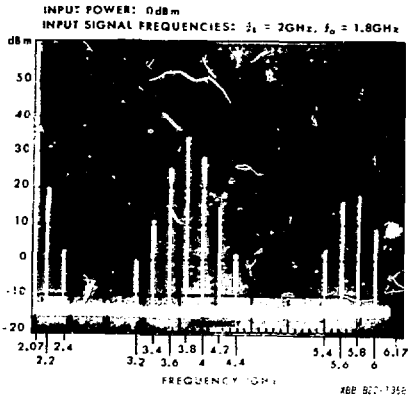

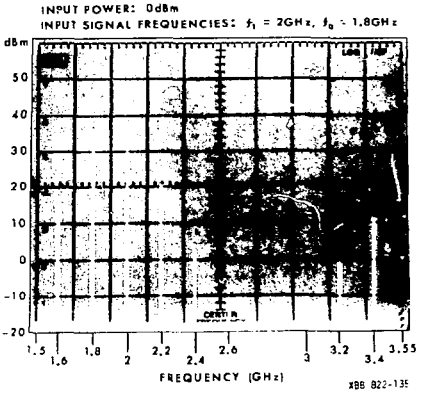

Fig. 12 Frequency spectrum display of the 2-4 GHz traveling-wave tube amplifier output signal.

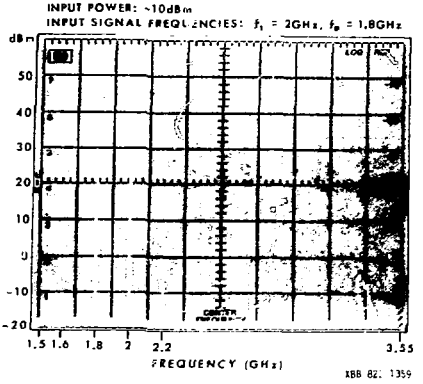

Fig. 14 Frequency spectrum display of the amplifier output signal.

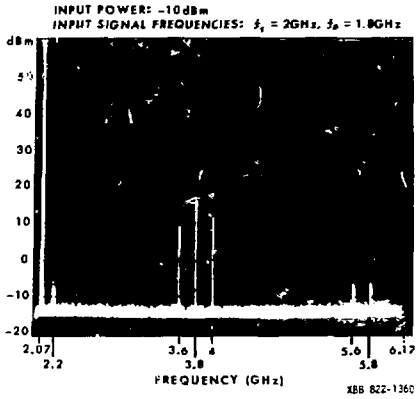

Fig. 15 Frequency spectrum display of the amplifier output signal.

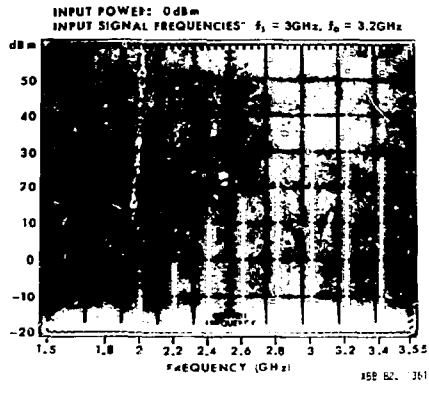

Fig. 17 Frequency spectrum display of the 2-4 GHz traveling wave tube amplifier output signal.

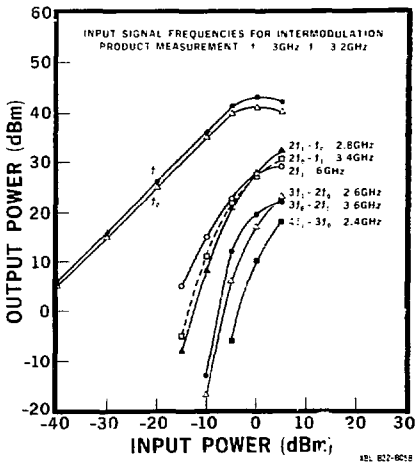

Fig. 16 Typical performance characteristics of the 2-4 GHz traveling wave tube amplifier.

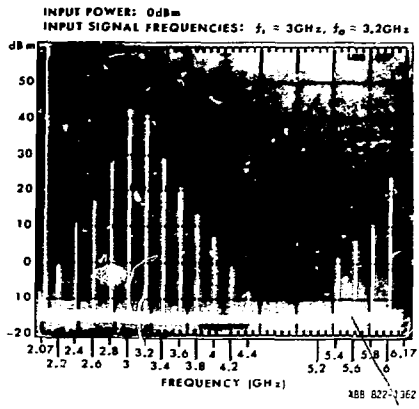

Fig. 18 Frequency spectrum display of the amplifier output signal.

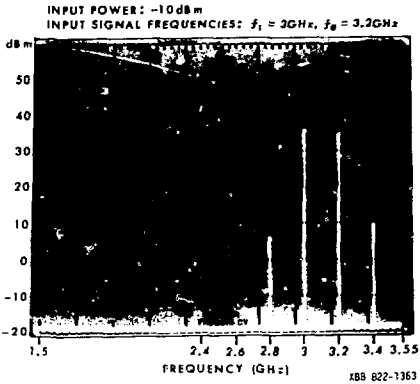

Fig. 19 Frequency spectrum display of the amplifier output signal.

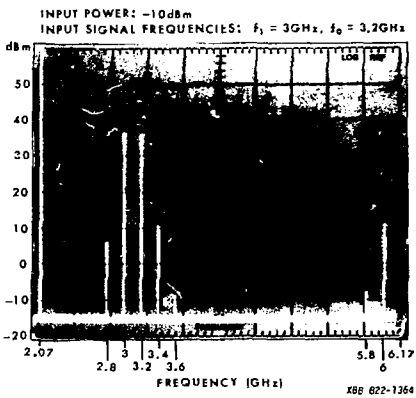

Fig. 20 Frequency spectrum display of the amplifier output signal.

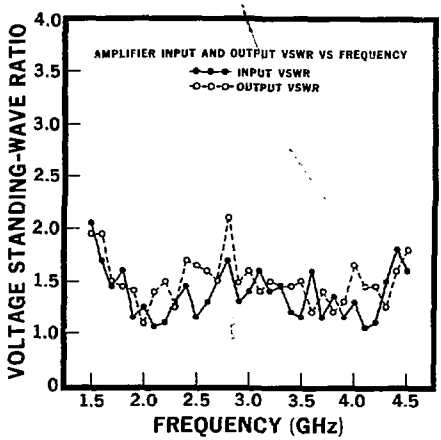

Fig. 21 Amplifier input and output voltage standing-wave ratio as a function of frequency.

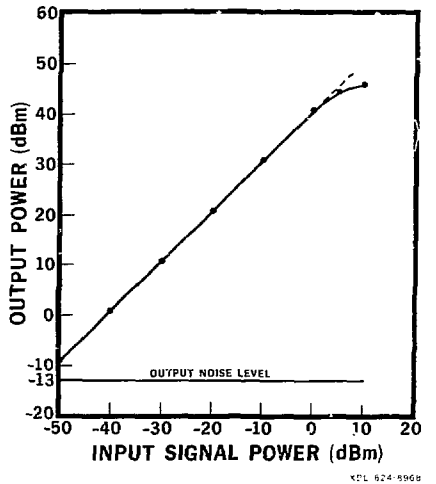

Fig. 22 Output noise power level as a function of the input noise power.

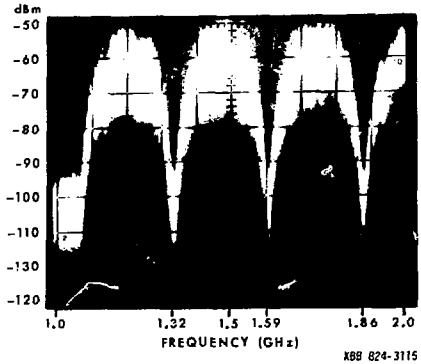

Fig. 23 Input noise spectrum.

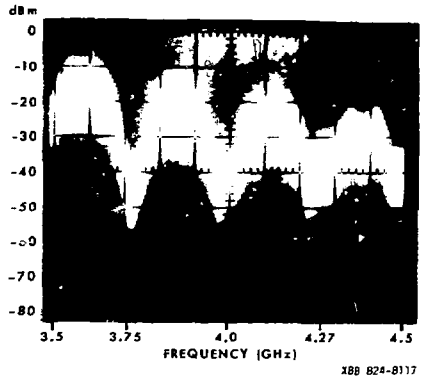

Fig. 25 Output noise spectrum of the amplifier.

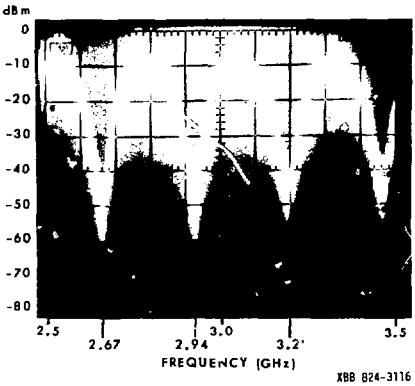

Fig. 24 Output noise spectrum of the amplifier.